Title: New method evaluating currents keeping the voltage constant for fast and highly resolved measurement of Arrhenius relation and capacity fade

Authors

Meinert Lewerenz^{a,b}, Stefan Käbitz^{b,c}, Marcus Knips^{a,b}, Jens Münnix^{a,b}, Johannes Schmalstieg^{a,b}, Alexander Warnecke^{a,b} and Dirk Uwe Sauer^{a,b,c}

Affiliation

- a) Electrochemical Energy Conversion and Storage Systems Group, Institute for Power Electronics and Electrical Drives (ISEA), RWTH Aachen University, Jägerstrasse 17/19, D-52066 Aachen, Germany
- b) Juelich Aachen Research Alliance, JARA-Energy, Germany
- c) Helmholtz Institute Münster (HI MS), IEK-12, Forschungszentrum Jülich, Corrensstrasse 46, 48149 Münster, Germany

Abstract

The evaluation of floating currents is a powerful method to characterize capacity fade induced by calendaric aging and enables a highly resolved representation of the Arrhenius relation. The test arrangement is simple and could constitute a cheap alternative to state-of-the-art calendaric aging tests including check-up tests. Therefore the currents to maintain a constant voltage are evaluated. This method is validated by analyzing nine cylindrical 8 Ah LiFePO₄|Graphite battery cells during calendaric aging at 25 °C, 40 °C and 60 °C at 3.6 V (100% SOC). The 3.6 V are kept by applying constant voltage while the floating currents are logged. The floating currents correlate with the rate of capacity loss measured during capacity tests. The floating currents reveal to be rather constant at 25 °C, linearly increasing at 40 °C and decreasing from a higher level at 60 °C. Additional tests with three test cells, with the temperature rising from 40 to 60 °C in steps of 5 K, exhibit non-constant currents starting from 50 °C on with high variations amongst the tested cells. Once stored above 50 °C, the cells exhibit increased floating currents compared to the measurement at the same temperature before exceeding 50 °C.

Key Words

Floating currents; LFP; LiPF6; calendaric aging; floating current analysis

Abbreviations

FCE: full cycle equivalents

EC: ethylene carbonate

DMC: dimethylene carbonate

EMC: ethylene-methylene carbonate

DEC: diethylene carbonate

LFP: lithium iron phosphate

SEI: solid electrolyte interphase

DOD: depth-of-discharge

SOC: state-of-charge

1. Introduction

Lithium-ion batteries are usually examined by means of cyclic aging or calendaric aging tests. The boundary conditions for calendaric aging are defined by the state-of-charge (SOC) or by the voltage of the cell and the ambient temperature [1][2]. Generally these factors are kept constant to be able to clearly determine if aging is caused by the SOC or by cell voltage and temperature.

The question whether the aging is path-invariant or not is hardly addressed in literature, where test conditions such as SOC and temperature are interchanged [2][3]. The answer to this question is quite useful to know, as the modeling of path-invariant aging can be implemented in a rate-based way. This is by far easier than if there is a path dependency with respect to temperature or SOC, where the aging rates depend on the cells' prehistory.

Furthermore there are two strategies to keep the SOC or voltage constant. Mostly the cells are just charged or discharged to a certain voltage level or SOC and then stored at a specific temperature (storage test) [4]. Sometimes they are floated, which means that the voltage is kept by a charger at a constant voltage level (float test) [1][5]. Float tests maintain a constant SOC recharging the battery and compensating self-discharge effects and side reactions [6]. During storage tests the cell voltage may decrease because of these processes, wherefore the aging tests will take place with a successively lower lithiated anode. The influence of floating the cell vs. open circuit storage tests is not clearly discussed in literature. Käbitz et al. [2] report that keeping the cell at constant voltage compared to open circuit voltage leads to a measureable difference only at 100% SOC as the aging rates at lower SOC do hardly differ. Nevertheless the floating current to keep the voltage is not or scarcely measured or evaluated. One example is the work of Zeng et al. [7], where the floating currents are evaluated at extremely high potentials of 4.5 V for a LiNi_{0.6}Mn_{0.2}Co_{0.2}O₂ cathode to measure the parasitic reactions at 30 °C ambient temperature.

The calendaric aging for lithium-ion batteries is described in literature to be strongly depending on the active material of the cathode and the anode, the coating quality, the electrolyte solvent, conductive salts, additives and any impurities as reported by Vetter et al.[8]. Thus calendaric aging tests on isolated components like the electrolyte are hardly sufficient to understand a complete cell arrangement and its aging. Commonly the calendaric aging of battery cells is characterized by capacity loss according to loss of active lithium and increase of internal resistance due to increasing solid-electrolyte-interphase (SEI) [9]. However, performing periodic check-ups including e.g. capacity and pulse tests converts any calendaric aging test to some extent into a cycle test. Therefore the check-up frequency has to be a compromise between time resolution and minimizing the checkup influence by extending the time in between the check-ups. Also a moderate temperature and a sufficiently low C-rate should be chosen for these tests to ensure that check-ups will most probably not contribute to aging.

It is challenging to compare calendaric aging tests from different publications if they are executed under different check-up conditions. Check-up tests can be influenced by reversible capacity effects like self-discharge [8] or compensation currents [6] that might be influenced by check-up frequency, C-rate and temperature. These reversible capacity effects are not easily separable by standard capacity tests.

Within this publication, a tool to measure floating currents is presented that in a steady state will solely return the pure loss of charge that is strongly correlated to loss of capacity or loss of active lithium respectively. Thus the capacity loss, the internal resistance and any reversible capacity effect can be separated. The reversible capacity effects can be observed in the transient effect at the beginning of the floating test before a steady state is reached. This part gives information about reversible capacity effects like the passive electrode effect presented in our previous publication [10]. Finally the floating currents are a good measurand to check the Arrhenius behavior as will be shown later.

2. Experimental

In the calendaric aging tests cylindrical 8 Ah cells with lithium iron phosphate (LFP) on the cathode side, graphite on the anode side and (EC-DMC-DEC-EMC)-LiPF₆ electrolyte were employed. They belong to a larger test set published before [10].

The cells are stored at three temperatures 25 °C, 40 °C and 60 °C and at a cell potential of 3.6 V, which corresponds to about 100% SOC. For each test condition, three cells are included. The accuracy of the temperature over time of the 110 I Memmert oven is +/- 0.2 K for all tests, measured with a temperature sensor positioned on the case of each cell.

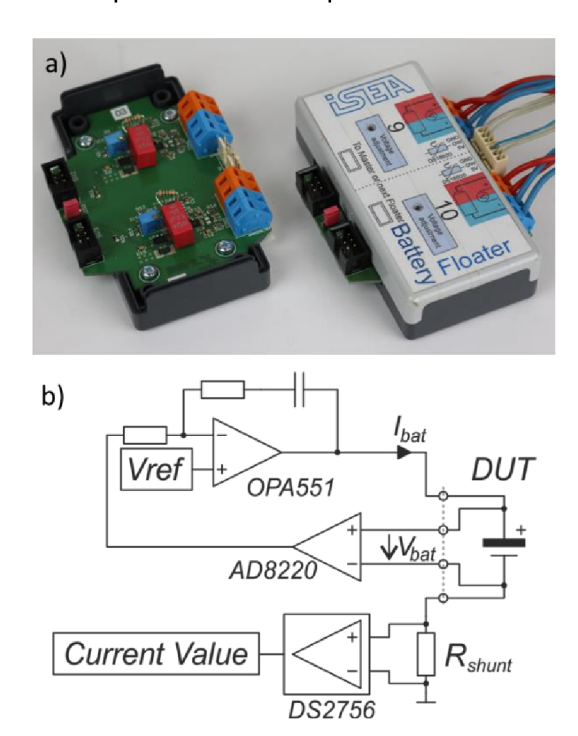


Figure 1 a) Photograph of the floater device comprising two floater units. b) Principle electronic sketch of the floater

The voltage is kept at 3.6 V +/- 2.5 mV by constant voltage charging utilizing a self-constructed battery floater that enables temperature measurement on the cell case (sensor type: DS18B20; precision: +/- 0.5 K), measurement and adjustment of the applied cell voltage, and a charging current source including high-precision measurement. This device will be referred to as 'floater' or 'floater unit' in the following. A picture of the floater device is shown in *Figure 1* a. One box includes two independent floater units and is able to connect two temperature sensors to capture the surface temperature of the battery. The costs for such a prototype are in the order of 100 € including two floater units.

Figure 1 b shows the principle schematic of the floater hardware. The battery is contacted with a four point connection to the floater. A high precision amplifier (AD8220) is used to measure the battery voltage. To keep the battery voltage constant at 3.6 V, a PI control loop with a large time constant is used. First of all, the measured battery voltage is stored in our logging system, so it is available for evaluation (not depict). Secondly, this voltage is the negative input of the battery sourcing amplifier (OPA551); the positive input is connected to a high-precision reference voltage, which is adjustable by a precision potentiometer. This is used to control both the battery voltage and the float voltage. The battery current or floating current is captured by means of a high-accuracy battery fuel gauge (DS2756). The resolution

of the measured current value amounts to 15 bit (one direction) and is averaged over 4096 values over 2.8 s. The maximum offset value is denoted as +/- 7.8125 $\mu V \cdot \Omega^{-1}$ and the current gain error as 1% of the actual value. The current is captured by a shunt resistor with a value of 1 Ω and an accuracy of 1%. The shunt resistor's temperature dependency is neglected. All in all, after an offset calibration, the floater unit is capable to measure float currents with a precision of 2% for currents greater than 100 μ A and with a maximum deviation of 1 μ A for currents smaller than 100 μ A.

To validate the precision of the floater, a reference measurement was accomplished. By this, instead of a battery, the currents over three simple resistors (18 k Ω , 39 k Ω and 220 k Ω) are measured with the floater unit and compared with the results of an Agilent 34401A 6.5 digits' multimeter with a specified precision of 2 μ A. Table 1 depicts the measured currents for a representative floater I (Floater) and a reference multimeter I (Agilent).

Table 1 Comparison of the measured currents between the self-constructed floater unit and an Agilent 34401A 6.5 digits' multimeter while connected to simple resistors.

Resistor [k Ω]	I _(Agilent) [μΑ]	I _(Floater) [μΑ]	ΔI [μ A]	ΔΙ [%]
220	16.5	17.6	-1.1	6.5
39	92.2	91.8	0.4	0.5
18	200.8	201.2	-0.4	0.2

With the stated resolution of the test setup, Table 1 shows a good accordance with the stated floater's precision. The floating currents' offset is corrected by measuring the current value in the unplugged state during the check-ups.

The floating currents necessary to maintain 3.6 V during aging are measured for each cell. Due to data logger problems no data between about day 300 and day 700 of the storage tests at 25 $^{\circ}$ C and 40 $^{\circ}$ C were recorded. However, as the trend of the floating currents follows a linear-like behavior, these tests may be simply interpolated, which will be described later in this publication.

The floating is interrupted for check-up tests after initially 14 days, and the period is reduced for slow aging conditions during testing time. At each check-up, a capacity test at 1 C and 0.25 C and a pulse test were performed.

The capacity test is executed in a temperature chamber (Binder MK53) at 25 °C with a variation of \pm 1. K using a Digatron MCFT 20-05-50ME test station with a precision of 0.1% of the current measurement. During the capacity test the discharged cells are charged with 1 C (8 A) up to 3.65 V, followed by constant-voltage charging down to I < 0.05 C (maximum 2 h). Afterwards the cells rest for 30 min before they are discharged with 1 C (8 A) until the cut-off voltage of 2.0 V is reached. The determination of the capacity test with 0.25 C (2 A) is performed analogously.

The pulse test is executed after a 30 min rest period at a SOC of 50% with respect to the actual capacity. The pulse test itself consists of a 18 s 2 C discharge pulse with a 40 s rest period, followed by a 10 s 1 C charge pulse with a subsequent 40 s rest period. In this publication the pulse tests are evaluated after 10 s at 50% SOC for discharge and referred to as internal resistance in the following sections.

3. Results and Discussion

3.1 Capacity and internal resistance

The capacity trend and the internal resistance of the cells kept at 100% SOC / 3.6 V with ambient temperatures of 25 °C, 40 °C and 60 °C were already shown by ourselves [10] and are displayed in Figure 2. A temperature-dependent increase of capacity fade is eye-catching while a good reproducibility is observable only up to 40 °C. Tests at 60 °C, by contrast, exhibit a higher spread of the three cells. A slightly stronger loss of capacity can be recognized for cell 6 in the left of Figure 2 compared to cells 4 and 5 at 40 °C tests, which will be important later when the floating currents are described.

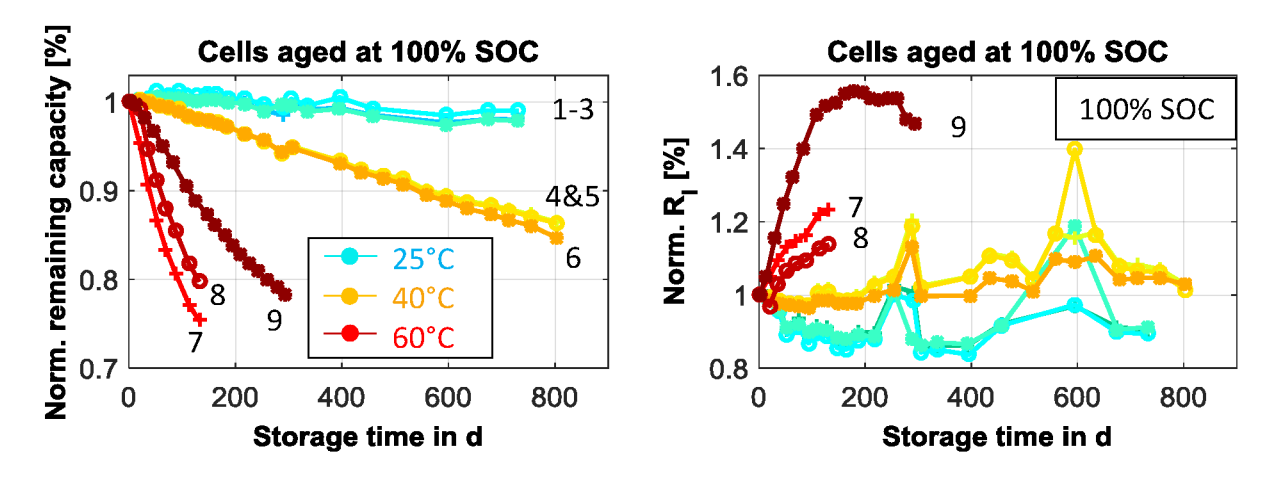


Figure 2 Illustration of the remaining capacity normalized to their initial capacity (left) and the internal resistance measured at 50% SOC normalized to their initial resistance (right) of all three cells of the calendaric test at 100% SOC at 25 $^{\circ}$ C, 40 $^{\circ}$ C and 60 $^{\circ}$ C.

The internal resistance decreases by 10% during the 25 °C tests; remains rather constant for the 40 °C tests and increases for the 60 °C tests. Cell 9 of the 60 °C test shows that even a saturated level for the internal resistance can be reached. In general the internal resistance curves in Figure 2 on the right return a few data points that do not follow the overall trend. At day 250 the chamber temperature was set wrongly to 23 °C instead of 25 °C, and at day 600 one cell of the 25 °C and 40 °C tests respectively exhibited most probably a measurement error as no specific reason for the increase could be found. These deviations correspond to the high sensitivity of the cells to temperature changes during the check-up tests and are not related to aging. Notably the cell with the highest resistance increase has the lowest capacity loss rate.

3.2 Floating currents at constant temperatures

The floating currents convey two kinds of information: Reversible and irreversible loss of capacity. While the irreversible loss of capacity originates from loss of active lithium, the reversible loss of capacity includes self-discharge and charge compensation processes like the passive electrode effect.

The floating currents of the cells kept at 100% SOC / 3.6 V with ambient temperatures of 25 $^{\circ}$ C, 40 $^{\circ}$ C and 60 $^{\circ}$ C are displayed in Figure 4. A positive current represents charging of the cell. The floating condition is regularly interrupted by check-ups; this interruption causes the high floating currents occurring directly after each check-up. For 25 $^{\circ}$ C the floating

currents are comparably low and have a high measurement uncertainty with respect to the floater accuracy.

For the 25 °C and 40 °C tests the curve is zoomed to the first measurement intervals, as presented in Figure 3. During the first 200 days of aging the floating currents do not reach a steady state within the measurement period. The signal before reaching the steady state will be called the transient effect in the following. Astonishingly the different trends of cell 6 and cells 4 and 5 of the 40 °C test condition are recognizable from the start until the end of test, showing a correlation of higher capacity loss with higher floating charge currents. The curve shape of all cells is comparable. Thus, this difference seems to be induced by different aging of the cells.

The initial differences in the transient effect of the cells tested at 25 °C are already equalized within the first 100 days of aging. For these cells the transient effects in the first three storage periods exhibit a different shape and seem not to represent irreversible aging. This reversible effect can be explained by the trend based on the passive electrode effect presented in our previous publication [10] and by the group of Dahn [6]. The potential differences of the passive anode prior to test begin of about 80% SOC and the test SOC of about 100% SOC are both within the last plateau of the anode potential. They are therefore too low to generate a measurable lithium-ion flow. However, during check-up lower SOC are passed over, which induces a lithium-ion flow from the passive to the active part with comparably high potential differences especially at low SOC of the full cell. Starting the constant voltage phase of the floating test, the lithium-ions flow back to the passive anode with a low velocity as the potential differences at higher SOC are lower due to the flat potential curve of the anode. Finally, the differences of the three cells will most probably originate from the prehistory of the cells after manufacturing, such as different manufacturing dates or coating qualities of the anode overhang.

The compensation currents, resulting from the passive electrode effect, seem to be highest at begin of test and are successively vanishing. The reduction of this effect seems to be faster with increasing storage temperature. This is in good agreement with an upcoming publication where it will be shown that the lithium-ion transport between active and passive anode will be successively hindered by electrical particle disconnection or dry out of electrolyte at the begin of the anode overhang. The velocity, with which this lithium-ion flow is impeded, correlates with the capacity loss. More insight into this aging effect will be provided in a subsequent publication introducing the capacity difference analysis (CDA) that is currently under review [11].

According to the theory mentioned before, the steady-state value represents the irreversible aging, which is typically loss of active lithium for calendaric aging tests. Evaluating only the steady-state values for the entire aging time, given in Figure 4, the 25 °C tests remain constant at about 14 μ A in average. At 40 °C the floating current is linearly increasing starting with 70 μ A and ending after about two years at 100 μ A for cells 4 and 5, whereas cell 6 ends up at 135 μ A. The floating currents at 60 °C are significantly higher and show analogies to the capacity fade characteristics: a non-uniform course of the three different cells and furthermore a non-linear trend which, instead of a monotonously increasing course, rather exhibits a decreasing or constant course. In all cells tested at 60 °C and 100% SOC, a significant amount of the element Fe was found on the anode [10], which is probably the cause of the different aging pattern. Cells 7 and 8 aged at 60 °C show a comparable trend with respect to capacity fade and floating current. The floating currents start from 700-800 μ A

and decrease to $450\text{-}600~\mu\text{A}$ at the end of the test. Cell 9 shows a different trend where the floating current is finally increasing before it stays rather constant in a current window of $250\text{-}340~\mu\text{A}$ until the end of test. The differences of cell 9 compared to cells 7 and 8 could result from different coating qualities (porosity, homogeneity and impurities) and thus SEI quality. In the end it is very hard to measure and quantify the quality of the coating.

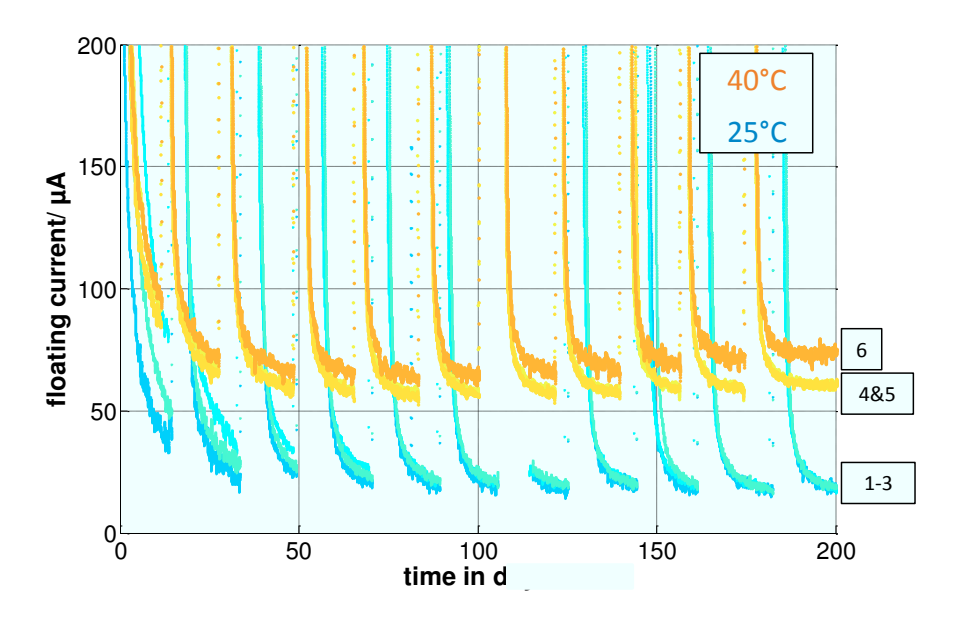


Figure 3 Diagram of the measured floating currents for 25 °C and 40 °C within the first 200 days of aging.

3.3 Correlation of floating currents

3.3.1 Comparison by differentiation of capacity tests

At first the correlation between the trend of the floating currents and the rate of capacity fade dQ dt⁻¹ is checked. For this purpose the resulting values of the differentiation of the 0.25 C-capacity tests are plotted as shown in Figure 5.

The courses of the curves in Figure 4 and Figure 5 reveal a certain correlation among each other, whereas the derivative of the capacity trend is quite noisy at 25 and 40 °C as the aging is relatively low compared to the temperature chamber regulation. It can therefore not be concluded, that the slightly increasing trend of the 40 °C floating current is also reflected by the capacity loss slope. Although the correlation between the floating currents and the capacity fade rate cannot be concluded via Figure 4 and Figure 5, cell 6 of the test batch reveals a higher floating current which correlates with a higher capacity loss as can be seen in the standard capacity representation in Figure 2.

In addition, the passive electrode effect will lead to an increase of extractable capacity, while this increase will be completely separable evaluating only the steady-state floating currents [6] [10]. The increased internal resistance especially at 60 °C will lead to a higher rate of capacity fade, whereas the effect on the floating currents will be negligible due to the very low currents measured. After all, without knowing any absolute values for these effects, the two methods mentioned cannot be compared unequivocally.

Monitoring the aging via capacity tests includes a lower aging rate during the capacity test itself, caused by a mostly lower ambient temperature and lower SOC during checkup. The floating current, in contrast, only returns the aging rate at the specific moment. As the check-

up periods are in the order of 10% of the entire testing time, the lower aging during check-up becomes relevant and has to be taken into account. For an accurate comparison the effective floating currents need to be calculated by determining the weighted average of floating currents during aging and during check-up over the entire testing time including the check-up periods. For the first approach, the floating currents of the 25 °C floating tests are used to calculate the aging during the capacity tests.

Therefore the correlation between capacity loss and floating current is optimized in the following chapter by including low aging periods during check-up to determine the effective floating current with respect to floating test results.

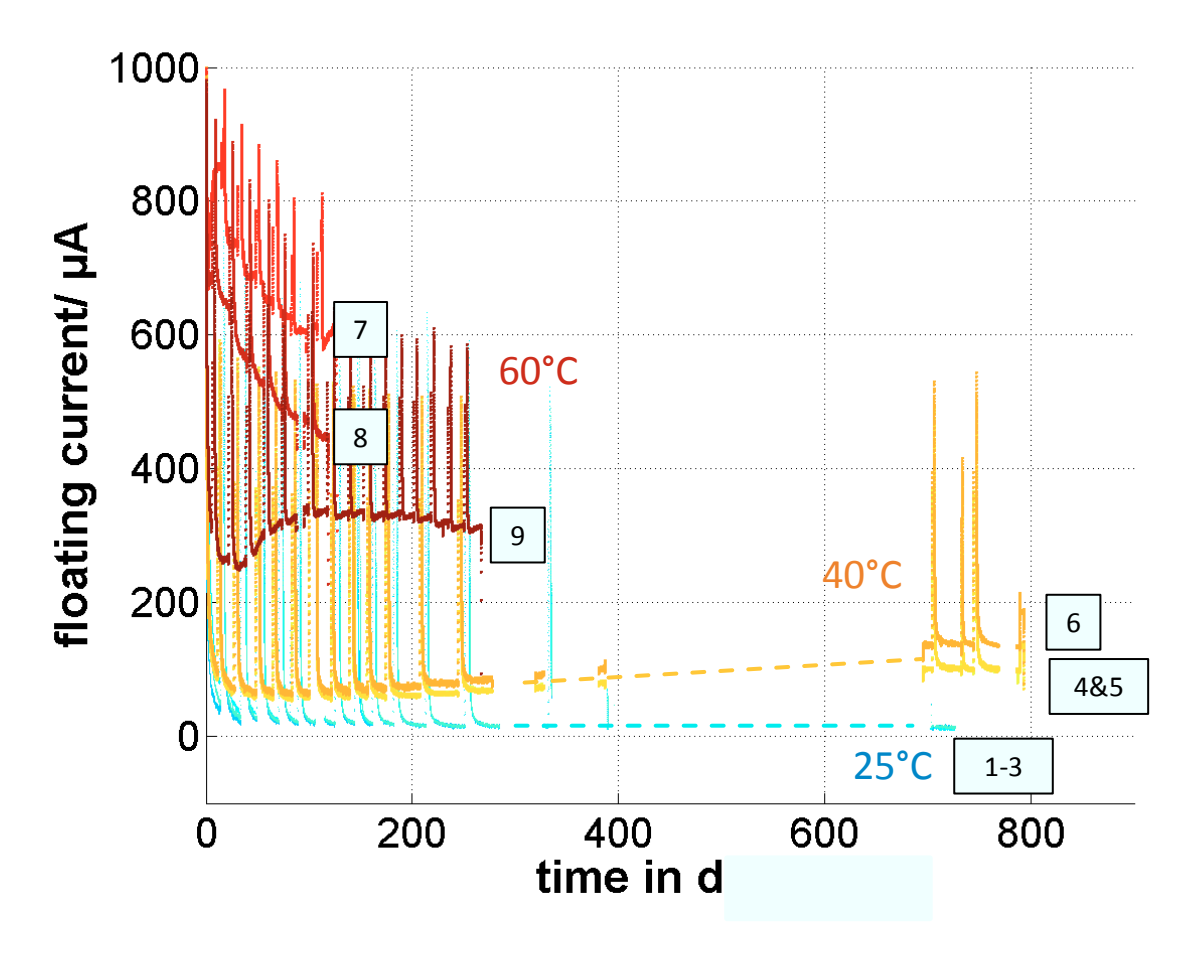


Figure 4 Illustration of the floating currents to keep the cell at 3.6 V. All recorded current-data are smoothed for a better overview. Positive floating currents represent charging currents of the cell. As after a check-up and a full charge of the cells the floater is reconnected, the current is declining until the cell approaches a rather steady state. Unfortunately, periods with no signal from 300-700 days could not be logged due to problems with the logging system. The missing data of the 25 °C and 40 °C seem to be well interpolated linearly which is sketched in the illustration with a dashed line.

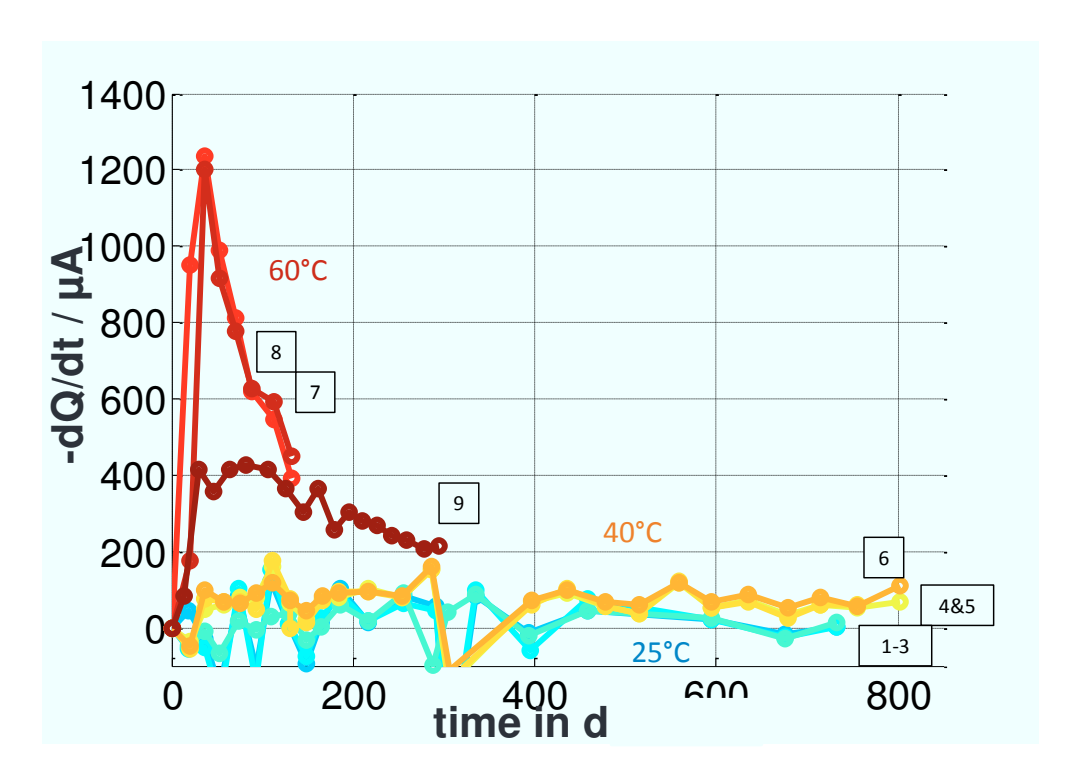


Figure 5 Illustration of the derivative of the capacity trend dQ df¹, measured at 0.25 C over aging time for all tests. The results for the 25 °C and 40 °C tests are quite noisy due to the relatively high influence of the temperature stability within the check-up, compared to the very slow aging rates of these tests.

3.3.2 Comparison using total absolute capacity loss

As a next step, the floating current and the capacity fade are compared by their start and end values. For this comparison the course of the aging is not taken into account. The average floating currents I_{float}^{avg} for each test cell are calculated according to formula 1:

$$I_{float}^{avg} = \frac{I_{float}^{aging} \cdot t_{float}^{aging} + I_{float}^{Check-up} \cdot t_{float}^{Check-up}}{t_{float}^{aging} + t_{float}^{Check-up}}$$
(1)

Here the mean floating current I_{float}^{aging} of the entire aging test is multiplied by the duration of the aging test t_{float}^{aging} . Additionally, in a first approach a mean floating current during the check-ups is assumed to be 14 μ A according to the test results at 25 °C, and multiplied by the duration of all check-ups $t_{float}^{Check-up}$. The weighted average of both floating currents adds up to I_{float}^{avg} . All values are given in Table 2.

Table 2 Measured data of averaged floating currents I_{float} and aging time t_{float} during aging and check-up. Thereafter the I_{float}^{avg} and ΔQ_{float}^{total} are calculated.

	I_{float}^{aging}	t_{float}^{aging}	$I_{float}^{Check-up}$	$t_{float}^{\mathit{Check-up}}$	I_{float}^{avg}	ΔQ_{float}^{total}
	μA	d	μA	d	μΑ	Ah
25°C-1-3	13-15	661		70	14	0.25
40°C-4/5	70	727		75	65	1.25
40°C-6	89	727			82	1.58
60°C-7	680	111	14	21	574	1.82
60°C-8	553	111		21	467	1.48
60°C-9	320	240		54	264	1.86

Next the capacity tests are evaluated. The value I_{float}^{calc} for the capacity tests represents the equivalent floating current and is determined according to formula 2:

$$I_{float}^{calc} = \frac{\Delta Q^{total}}{\Delta t^{total}}(2)$$

Therefore the absolute capacity loss ΔQ^{total} is divided by the total aging time Δt^{total} . Alternatively the total capacity loss ΔQ^{total}_{float} is calculated analogously and can be compared to the measured capacity loss ΔQ^{total} .

In Table 3 the calculated average floating current I_{float}^{calc} and the total capacity loss ΔQ^{total} of the floating tests are given as well as the capacities measured at 0.25 C and 1 C.

The results show a good correlation with respect to floating currents with a deviation of 3-5 μ A corresponding to a 3-18% relative deviation between the floating currents and the 0.25 C capacity tests. The maximum absolute deviation at 25 °C and 40 °C of 5 μ A is quite a good result as there are a lot of assumptions included and the impact of the passive electrode effect and the internal resistance cannot be excluded from standard capacity measurements. At 60 °C the differences are larger, which is quite plausible considering that the floating currents are not in a steady state and aging at temperatures higher than 50 °C increases the aging rates permanently at lower temperatures during the check-ups, which will be shown in the following chapter. Thus, the likely increased floating currents during check-up for the 60 °C test cells are not included in the assumptions for the effective floating current I_{float}^{avg} .

The deviations of the capacity tests at 1 C exhibit once more that the floating currents do not include effects due to internal resistance and passive electrode effect. Thus the capacity determined at the lowest C-rate will have the lowest deviations from the measured floating currents. To sum up, the steady state of each floating interval seems to represent the loss of active lithium excluding any information about the internal resistance. For future comparisons to other cells with different capacities, the floating current should be normalized to the nominal capacity comparable to the definition of C-rates.

Table 3 shows the measured or calculated floating currents I_{Float} and the total measured capacity loss ΔQ^{total} measured at 0.25 C and 1 C capacity tests and during floating tests. $\Delta \%$ returns the relative deviation of floating current I^{avg}_{float} and the I^{calc}_{float} measured at the corresponding C-rate.

-	Floating test results		0.25 C Capacity test results			1C Capacity test results		
	I_{float}^{avg}	ΔQ_{float}^{total}	I_{float}^{calc}	ΔQ^{total}	$\Delta\%$	I_{float}^{calc}	ΔQ^{total}	$\Delta\%$
	μΑ	Ah	μΑ	Ah		μΑ	Ah	
25°C-1-3	14	0.25	17	0.30	+18%	10	0.17	-40%
40°C-4/5	65	1.25	67	1.29	+3%	58	1.12	-12%
40°C-6	82	1.58	77	1.47	-6%	69	1.33	-19%
60°C-7	574	1.82	714	2.26	+20%	643	2.04	+11%
60°C-8	467	1.48	609	1.93	+23%	545	1.73	+14%
60°C-9	264	1.86	281	1.98	+6%	256	1.80	-3%

3.4 Floating current at variable temperatures

To visualize the transition of the rising floating currents at 40 °C and the significantly higher and rather constant or decreasing floating currents at 60 °C, an additional test is performed

(Figure 6). For this, three cells are used that had already been subject to our previous test at 25 °C. For these cells kept at 3.6 V for about two years no transient effect caused by compensation flow with respect to the anode overhang and residual charging after the checkup is expected anymore. During the test the temperature is increased from 40 °C up to 65 °C in steps of 5 °C at 3.6 V cell potential. Capacity tests are only performed initially at 25 °C and 40 °C. Up to 45 °C, all three cells are not distinguishable with respect to floating currents. From 50 °C on the three cells do not show a comparable behavior anymore and the floating currents are diverging at a constant temperature. Thus it seems as if another mechanism is dominating the aging that might be related to other battery constraints like residual moisture or Fe dissolution. This observation gets along with Lux et al. [12] who report that from 50 °C on the decomposition of the conductive salt LiPF₆ is dominating and strongly affects the SEI by forming hydrofluoric acid (HF).

Table 4 Floating currents maintaining 3.6 V for the three test cells measured at 45 °C before and after heating up to 65 °C (see also Figure 6).

	Before heating	After heating	After heating
	Day 30 (45 °C)	Day 80 (45 °C)	Day 117 (45 °C)
Cell 1	81 μΑ	167 μΑ	201 μΑ
Cell 2	80 μΑ	115 μΑ	133 μΑ
Cell 3	85 μΑ	190 μΑ	229 μΑ

This aging is irreversible as a temperature reduction back to 40 °C does not lead to a floating current comparable to the one measured before, an occurrence which cannot simply be explained by aging, taking the low aging rate of 40 °C tests into account as displayed in Figure 4. Results of the floating currents measured at 45 °C before and after heating up the cell are summarized in Table 4, and the floating currents for cell 1 are illustrated in Figure 7 to visualize the path-invariance of the floating currents with respect to variation of the temperature profile. It seems that the chemical environment of decomposed electrolyte within the battery is more aggressive to the SEI layer and causes aging with a stronger rate, or the stability of the SEI is considerably weakened by the high temperatures.

Finally the results refer to a path-invariant aging below 45 °C and a non-invariant aging above 50 °C. Thus, starting aging at temperatures higher than 50 °C and then reducing the temperature below 45 °C will lead to higher overall aging compared to starting aging at temperatures lower than 45 °C and increasing afterwards above 50 °C, as the floating currents in the low temperature phase will be increased due to the previously high temperature phase in the first scenario.

For the 60 °C test cell this result is supported by the fact that the calculated floating currents for the 0.25 C measurements are significantly higher than the measured effective floating currents, leading to the assumption of a low and constant floating current of 14 μ A during check-up. Therefore the floating currents during check-up will be presumably increased for the 60 °C tests.

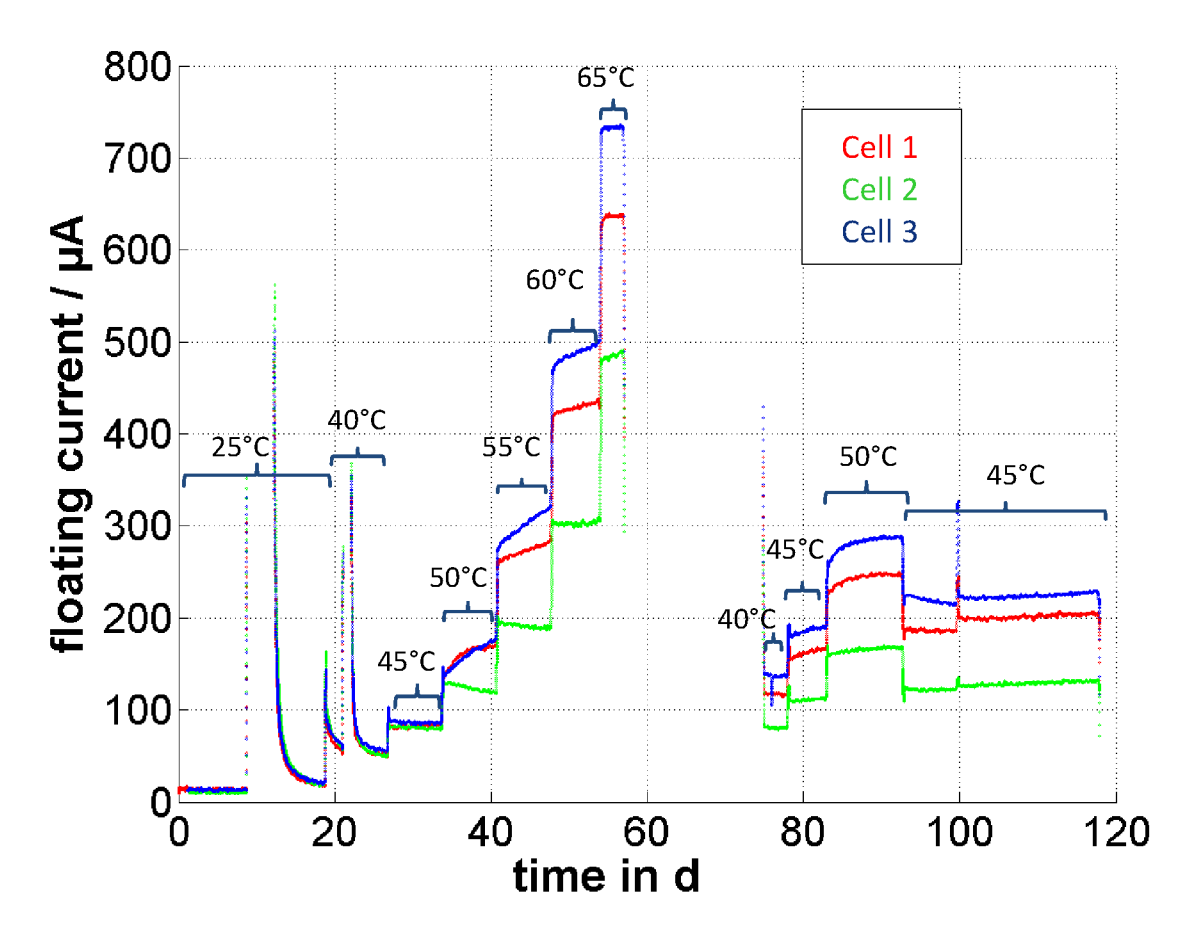


Figure 6 Illustration of the floating currents of three cells kept at 3.6 V and a varying temperature from 25 °C up to 65 °C.

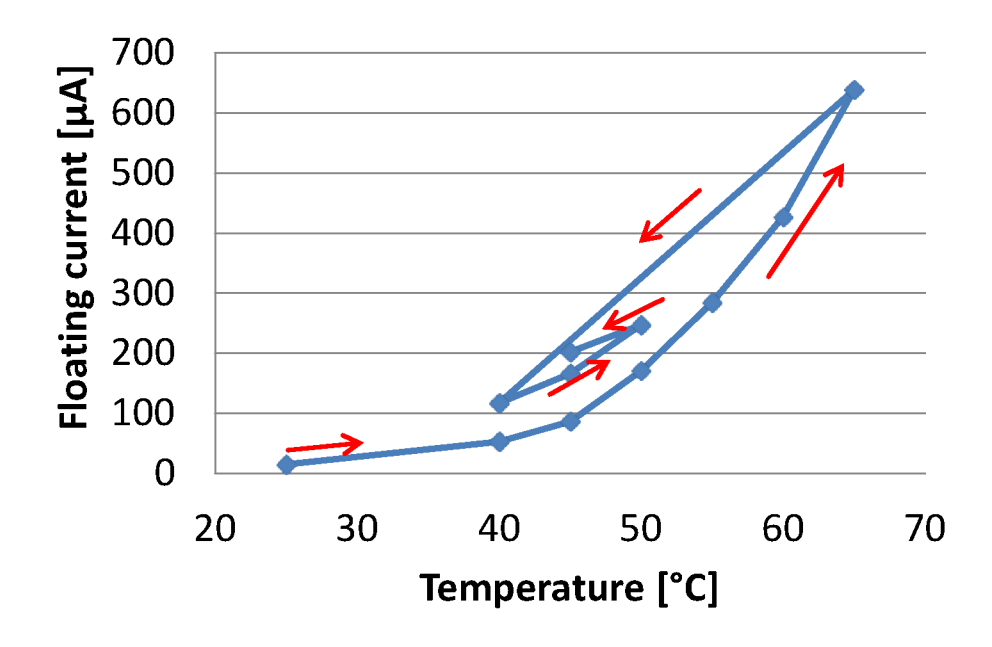


Figure 7 Illustration of the path-dependence based on the example of cell 1.

3.5 Arrhenius relation

If the aging processes at $25 \,^{\circ}\text{C}$, $40 \,^{\circ}\text{C}$ and $60 \,^{\circ}\text{C}$ were driven by the same aging mechanisms, they would have to follow the Arrhenius relation and return a linear trend in the Arrhenius plot. In Figure 8 on the left side the Arrhenius graph is given and a clear linear relation is obtained up to 130 days of aging and thereafter the capacity loss at $60 \,^{\circ}\text{C}$ starts to become slower. Finally, as the tests are performed only at three different temperatures, no further assumptions can be made according to this data.

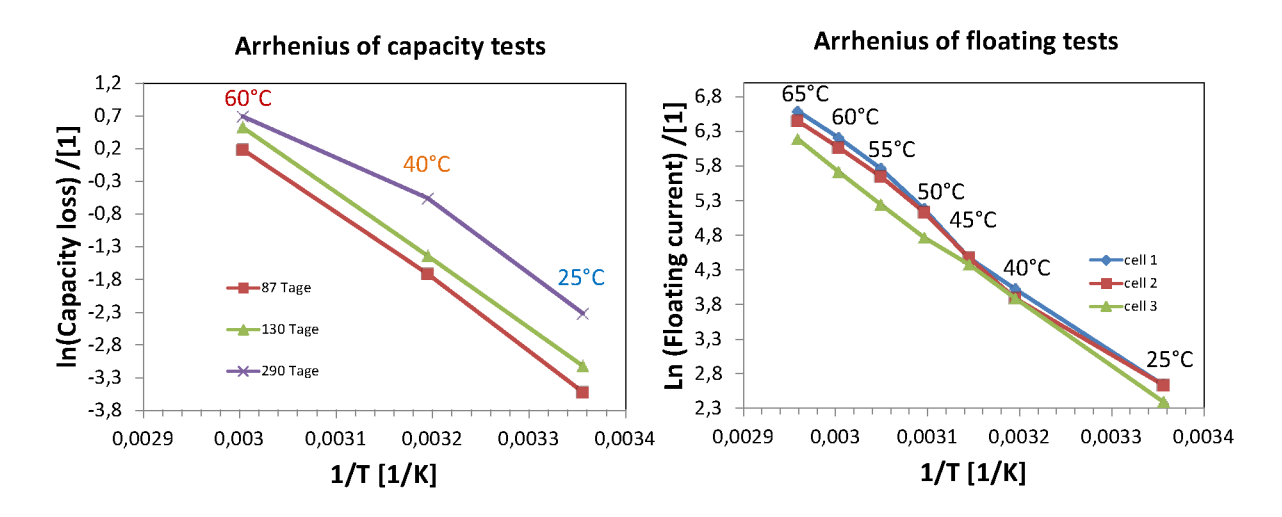


Figure 8 <u>Left</u>: Arrhenius plot of calendaric aged cells stored at 100% SOC at temperatures 25 °C, 40 °C and 60 °C. The time steps 87, 130 and 290 days are evaluated. <u>Right</u>: Arrhenius plot of three calendaric aged cells stored at 100% SOC at temperatures from 25 °C to 65 °C in smaller steps.

To get more information about different temperatures, the Arrhenius relation of the floating tests of three cells shown in Figure 6 is illustrated in Figure 8 on the right, whereby the last value for the floating current of each temperature step is evaluated. Astonishingly the Arrhenius relation is more or less fulfilled although the floating currents do not reach a steady state above 45 °C temperatures. Thus, the different aging mechanism below 45 °C and above 50 °C shown in the floating current analysis of the previous chapter are not observable in the Arrhenius plot.

3.6 Modelling of capacity fade

Assuming that the floating current correlates with the rate of capacity fade, the capacity fade reveals a constant linear decrease for 25 °C and a low pronounced quadratic decrease for 40 °C. At 60 °C the aging is quite non-uniform and is decreasing with aging. However, all of these measured trends do not follow a \sqrt{t} –function describing the protective nature of the growing solid electrolyte interphase (SEI) that is widely discussed in literature for example by Broussely et al. [5] and Ploehn et al. [13]. Thus the evaluation of the floating currents might enable to enhance the models describing the calendaric aging with respect to capacity fade.

Additionally the non-constant aging at elevated temperatures will help to establish more precise models of capacity fade.

4 Conclusions

Measurement and evaluation of floating currents exhibit valuable online information about aging of the cells with respect to pure capacity loss excluding influences of the internal resistance of the battery. The floating currents are in the order of a few μ A at 25 °C up to several 100 μ A at elevated temperatures as e.g. 60 °C. To be able to compare the floating currents with other battery cells, normalization with respect to the cells' capacity will be needed analogously to definition of C-rates. The floating currents are matching quite well to the rate of capacity loss measured at low current rates such as 0.25 °C. The deviations between those two methods can be found in internal resistance and in a transient effect that is caused most probably by the passive electrode effect or self-discharge. Evaluating the floating currents enables separating the reversible capacity trend of the passive electrode effect from the actual capacity fade.

Applying the floating current to a cell while varying the temperature provides detailed information about the chemical stability of the whole cell system. Thus the temperature window with a quite reasonable capacity loss can be obtained for various applications. For this case another aging process is dominating starting between 45-50 °C that reveals big differences considering cells that show a non-distinguishable behavior up to 45 °C. Thus aging below 45 °C is path-invariant and starts to be path-depending above 50 °C. This theory is supported by the fact that the floating currents at 25 and 40 °C show either a constant or an increasing trend while tests at 60 °C reveal rather reducing floating currents with respect to progressing aging. The aging at 60 °C is associated with the presence of Fe found on the anode. Additionally, cells that behave similarly below 45 °C behave differently above 50 °C.

The evaluation of the capacity and the floating currents at 25, 40 and 60 °C according to Arrhenius law does not give any evidence that there are two different processes with significantly different activation energies below 45 °C and above 50 °C.

Summing up, the evaluation of floating currents is a cheap and highly resolved measurement technique that enables the analysis of the pure capacity loss excluding the internal resistance. Well specified parameterized aging helps modeling the loss of capacity, the increase of internal resistance and reversible effects (passive electrode effect) separately.

Acknowledgement

The results were generated in the framework of the projects MEET-HiEnD (03X4634B), Powerblock+ (01M3200E) and the research training group "mobilEM" (GRK 1856/1). We would like to thank the Bundesministerium für Bildung und Forschung (BMBF) and the DFG for funding and Yusuf Yuradgel for his technical support.

References

- [1] M. Ecker, N. Nieto, S. Käbitz, J. Schmalstieg, H. Blanke, A. Warnecke, D.U. Sauer, Calendar and cycle life study of Li(NiMnCo)O2-based 18650 lithium-ion batteries, J. Power Sources. 248 (2014) 839–851. doi:10.1016/j.jpowsour.2013.09.143.
- [2] S. Käbitz, J.B. Gerschler, M. Ecker, Y. Yurdagel, B. Emmermacher, D. André, T. Mitsch, D.U. Sauer, Cycle and calendar life study of a graphite|LiNi1/3Mn 1/3Co1/3O2 Li-ion high energy system. Part A: Full cell characterization, J. Power Sources. 239 (2013) 572–583. doi:10.1016/j.jpowsour.2013.03.045.

- [3] K.L. Gering, S. V. Sazhin, D.K. Jamison, C.J. Michelbacher, B.Y. Liaw, M. Dubarry, M. Cugnet, Investigation of path dependence in commercial lithium-ion cells chosen for plug-in hybrid vehicle duty cycle protocols, J. Power Sources. 196 (2011) 3395–3403. doi:10.1016/j.jpowsour.2010.05.058.
- [4] I.V. E. Sarasketa-Zabala, I. Gandiaga, L.M. Rodriguez-Martinez, Calendar ageing analysis of a LiFePO 4 / graphite cell with dynamic model validations: Towards realistic lifetime predictions, 272 (2014) 45–57. doi:10.1016/j.jpowsour.2014.08.051.
- [5] M. Broussely, S. Herreyre, P. Biensan, P. Kasztejna, K. Nechev, R.J. Staniewicz, Aging mechanism in Li ion cells and calendar life predictions, J. Power Sources. 97–98 (2001) 13–21. doi:10.1016/S0378-7753(01)00722-4.
- [6] B. Gyenes, D.A. Stevens, V.L. Chevrier, J.R. Dahn, Understanding Anomalous Behavior in Coulombic Efficiency Measurements on Li-Ion Batteries, J. Electrochem. Soc. 162 (2015) A278–A283. doi:10.1149/2.0191503jes.
- [7] X. Zeng, G.L. Xu, Y. Li, X. Luo, F. Maglia, C. Bauer, S.F. Lux, O. Paschos, S.J. Kim, P. Lamp, J. Lu, K. Amine, Z. Chen, Kinetic study of parasitic reactions in lithium-ion batteries: A case study on LiNi0.6Mn0.2Co0.2O2, ACS Appl. Mater. Interfaces. 8 (2016) 3446–3451. doi:10.1021/acsami.5b11800.
- [8] J. Vetter, P. Nov, M.R. Wagner, C. Veit, Ageing mechanisms in lithium-ion batteries *α*, 147 (2005) 269–281. doi:10.1016/j.jpowsour.2005.01.006.
- [9] M. Kassem, C. Delacourt, Postmortem analysis of calendar-aged graphite/LiFePO4 cells, J. Power Sources. 235 (2013) 159–171. doi:10.1016/j.jpowsour.2013.01.147.
- [10] M. Lewerenz, J. Münnix, J. Schmalstieg, S. Käbitz, M. Knips, D.U. Sauer, Systematic aging of commercial LiFePO4jGraphite cylindrical cells including a theory explaining rise of capacity during aging, J. Power Sources. 345 (2017) 254–263. doi:10.1016/j.jpowsour.2017.01.133.
- [11] M. Lewerenz, A. Warnecke, D.U. Sauer, Introduction of capacity difference analysis (CDA) for analyzing lateral lithium-ion flow to determine the state of covering layer evolution, J. Power Sources. 354. (2017) 157–166. doi:10.1016/j.jpowsour.2017.04.043.
- [12] S.F. Lux, I.T. Lucas, E. Pollak, S. Passerini, M. Winter, R. Kostecki, The mechanism of HF formation in LiPF6 based organic carbonate electrolytes, Electrochem. Commun. 14 (2012) 47–50. doi:10.1016/j.elecom.2011.10.026.
- [13] H.J. Ploehn, P. Ramadass, R.E. White, Solvent Diffusion Model for Aging of Lithium-Ion Battery Cells, J. Electrochem. Soc. 151 (2004) A456. doi:10.1149/1.1644601.